International Journal of Power Electronics and Drive Systems (IJPEDS)
Vol. 15, No. 3, September 2024, pp. 1387~1398
ISSN: 2088-8694, DOI: 10.11591/ijpeds.v15.i3.pp1387-1398

Enhancing the efficiency of a dual three-phase permanent magnet synchronous motor with modified switching table for direct torque control

Fouad Labchir[1], Aziz El Afia[2], Karim Benkirane[1], Mohamed Khafallah[1]
[1]Department of Electrical Engineering, National High School of Electricity and Mechanics (ENSEM), Hassan II University, Casablanca, Morocco
[2]Department of Electrical Engineering, National High School of Arts and Crafts (ENSAM), Hassan II University, Casablanca, Morocco

Article Info

Article history:

Received Dec 28, 2023
Revised Mar 2, 2024
Accepted Mar 21, 2024

Keywords:

DTC
DTP-PMSM
Flux
New distribution of sectors
Stator current
Switching table
Vector space decomposition

ABSTRACT

Conventional direct torque control (DTC) can be served to drive a dual three-phase permanent magnet synchronous motor (DTP-PMSM) by controlling the torque and speed. It relies on the direct application of controlled sequences through the use of a combination of dual hysteresis controllers with a transitioning table. In the course of conventional DTC implementation, there's generation of high armature current with lower-level harmonics, leading to increased losses that affect the machine's effectiveness. To enable a diminishment in these harmonics and consequently enhance the motor's efficiency, an approach to modify the conventional DTC is proposed. Specifically, this strategy involves adapting a new distribution of sectors and substituting the elements of the obtained switching table with synthetic elements. Simulated data validate the effectiveness of the chosen methodology.

Corresponding Author:

Fouad Labchir
Department of Electrical Engineering, National High School of Electricity and Mechanics (ENSEM)
Hassan II University
Casablanca, Morocco
Email: fouadlabchir69@gmail.com

1. INTRODUCTION

In recent times, polyphase machines have gained significant attention for several compelling reasons: i) They enable power segmentation, facilitating the production of high-power machine converter assemblies with smaller gauge components; ii) They effectively reduce electromagnetic torque ripples and rotor losses; and iii) They enhance reliability by enabling correct operation even in degraded conditions with one or more open phases.

Among this apparatus, the dual three phase permanent magnet synchronous motor (DTP-PMSM) has arisen like a crucial element in the industrial sector, particularly in electric motorization for high-power applications such as railway traction or naval propulsion [1]–[7]. A control technique called field-oriented control (FOC) employing the vector space decomposition (VSD) method was explored in previous study [7]. Additionally, an alternative control strategy known as direct torque control (DTC) was arising in the mid-1980s by Takahashi [8], aiming to overcome the limitations of vector control. Unlike vector control, DTC involves separate regulation of torque and stator flux, enabling a decoupled imposition of torque and flux [9]. DTC has proven its ability to achieve advanced management of three-phase electrical propulsion systems [10].

When implementing conventional DTC on the DTP-PMSM, notable harmonic stator currents are often detected, leading to stator losses, and consequently a decline in the apparatus's overall effectiveness. In line with the VSD approach, the conventional DTC lacks the capability to manage the harmonics that manifest in the plane (z_1, z_2).In order to enhance conventional DTC, a modified DTC approach is proposed in [11], for the synchronous motor with five phases. This strategy involves selecting the appropriate voltage in two steps using a switching table. Further studies have been conducted to improve DTC by employing synthetic vectors in [12], [13]. Another alternative method proposed in [14] selects voltage elements built upon the flux stance in the (z_1, z_2) subspace, akin to the (α, β) subspace.

Our contribution is to enhance the efficiency of the DTP-PMSM by applying an approach that involves modifying the conventional DTC. To achieve this goal, the following plan is adopted for the rest of this document: i) Section 2 describes the motor model using the vector space decomposition (VSD) approach; ii) Section 3 covers the modeling of the motor power supply and present the conventional DTC approach, in the context of the search method; iii) Section 4 introduces the proposed modified DTC approach; iv) Section 5 the simulation results from both methods are showcased in order to confirm the efficacy of the proposed technique; and v) Finally, section 6 provides the conclusion of the article.

2. DTP-PMSM MODELING

To facilitate the analysis of the motor being examined [15], [16], the subsequent assumptions are taken into account: i) the motor operates without saturation, ii) iron losses are not considered, iii) the electromotive force (EMF) follows a sinusoidal pattern, and iv) effects of Foucault currents and hysteresis losses are minimal. Figure 1 provides a depiction of the DTP-PMSM model.

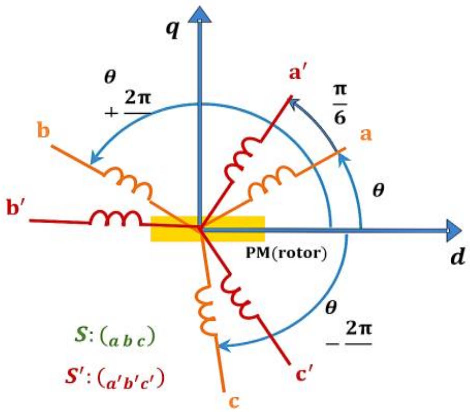

Figure 1. The DTP-PMSM windings

Electrical equation shown in (1) and (2).

$$(\mathrm{Vsabc}) = (\mathrm{Rs})(\mathrm{Isabc}) + \frac{d}{dt}(\Phi\mathrm{sabc}) \tag{1}$$

$$(\mathrm{Vsa'b'c'}) = (\mathrm{Rs})(\mathrm{Isa'b'c'}) + \frac{d}{dt}(\Phi\mathrm{sa'b'c'}) \tag{2}$$

Magnetic equation shown in (3) and (4).

$$(\Phi\mathrm{sabc}) = (\mathrm{Ls})(\mathrm{Isabc}) + (\Phi\mathrm{fabc}) \tag{3}$$

$$(\Phi\mathrm{sa'b'c'}) = (\mathrm{Ls})(\mathrm{Isa'b'c'}]) + (\Phi\mathrm{fa'b'c'}) \tag{4}$$

Mechanical equation shown in (5)-(7).

$$\mathrm{J}\, d\Omega/dt = \mathrm{Ce} - \mathrm{Cr} - \mathrm{Cf} \tag{5}$$

$$\mathrm{Ce} = \mathrm{Ce1} + \mathrm{Ce2} \tag{6}$$

$$\mathrm{Cf} = \mathrm{f} \times \Omega \tag{7}$$

With: i) Ce: electromagnetic torque, ii) Cr: load torque, iii) J: inertia moment, iv) **Ω**: rotor rotation speed, and v) f: friction viscous coefficient.

The development of a functional control system becomes achievable with the VSD model [17], utilizing the decoupling transformation matrix represented as (8).

$$T = \frac{1}{\sqrt{3}}\begin{pmatrix} 1 & -\frac{1}{2} & -\frac{1}{2} & -\frac{\sqrt{3}}{2} & \frac{\sqrt{3}}{2} & 0 \\ 0 & \frac{\sqrt{3}}{2} & -\frac{\sqrt{3}}{2} & \frac{1}{2} & \frac{1}{2} & -1 \\ 1 & -\frac{1}{2} & -\frac{1}{2} & -\frac{\sqrt{3}}{2} & \frac{\sqrt{3}}{2} & 0 \\ 0 & -\frac{\sqrt{3}}{2} & \frac{\sqrt{3}}{2} & \frac{1}{2} & \frac{1}{2} & -1 \\ 1 & 1 & 1 & 0 & 0 & 0 \\ 0 & 0 & 0 & 1 & 1 & 1 \end{pmatrix} \tag{8}$$

The process of decoupling transformation enables the simplification of intricate systems by breaking them down into three perpendicular subspaces: the torque components (α, β), (z_1, z_2) corresponds to the harmonic components, while (o_1, o_2) represents the zero-sequence [18]–[24]. The subsequent relationship remains accurate, as in (9).

$$\left(V_\alpha V_\beta V_{z1} V_{z2} V_{01} V_{02}\right)^{t} = \mathrm{T}\left(V_a V_b V_c V_{a'} V_{b'} V_{c'}\right)^{t} \tag{9}$$

The equations for the variables can be expressed in stationary frame as in (10)-(12).

$$\left(V_{\alpha\beta}\right) = \left(R_s\right)\left(i_{\alpha\beta}\right) + \frac{\mathrm{d}}{\mathrm{dt}}\left(\Psi_{\alpha\beta}\right) = \left(R_s\right)\left(i_{\alpha\beta}\right) + \frac{\mathrm{d}}{\mathrm{dt}}\left[\left(L_{\alpha\beta}\right)\left(i_{\alpha\beta}\right) + \Psi_{\mathrm{PM}}.\begin{pmatrix}\cos\theta \\ \sin\theta\end{pmatrix}\right] \tag{10}$$

$$\left(V_{z_{1,2}}\right) = \left(R_s\right)\left(i_{z_{1,2}}\right) + \frac{\mathrm{d}}{\mathrm{dt}}\left(\Psi_{z_{1,2}}\right) = \left(R_s\right)\left(i_{z_{1,2}}\right) + \left(L_z\right)\frac{\mathrm{d}}{\mathrm{dt}}\left(i_{z_{1,2}}\right) \tag{11}$$

$$\left(V_{o_{1,2}}\right) = \left(R_s\right)\left(i_{o_{1,2}}\right) + \frac{\mathrm{d}}{\mathrm{dt}}\left(\Psi_{o_{1,2}}\right) = \left(R_s\right)\left(i_{o_{1,2}}\right) + \left(L_o\right)\frac{\mathrm{d}}{\mathrm{dt}}\left(i_{o_{1,2}}\right) \tag{12}$$

Where:

$$\left(L_{\alpha\beta}\right) = \begin{pmatrix} \frac{(L_d + L_q)}{2} + \frac{(L_d - L_q)}{2}cos\ 2\theta & \frac{(L_d - L_q)}{2}sin\,2\theta \\ \frac{(L_d - L_q)}{2}sin\,2\theta & \frac{((L_d + L_q)}{2} - \frac{((L_d - L_q)}{2}cos\ 2\theta \end{pmatrix}$$

L_d, L_q denote the direct-axis and quadrature-axis inductances. L_z, L_o denotes stator self-leakage inductance after transformation.Ψ_{PM}: the magnetic flux linked by the permanent magnet.θ: the angle representing the rotor's position.

In line with the VSD technique outlined in study [17], the subspace that encompasses the (α, β) components includes both the fundamental component and harmonics. These harmonics are characterized by an order of 12Kth ± 1, where K takes on values like 1, 2, 3, and so forth. In a similar vein, harmonics exhibiting an order of 6Kth ± 1, where K follows a sequence of 1, 3, 5, and so on, are located within the plane (z_1, z_2). Furthermore, the harmonics with an order of 3Kth, where K follows the pattern 1, 3, 5, and so on, undergo a transformation into the zero-sequence subspace represented by (o_1, o_2).

The current components within the (α, β) subspace play a role in converting electromechanical energy. In contrast, the components found in both the (o_1, o_2) and (z_1, z_2) subspaces consist entirely of harmonics. These harmonics do not actively participate in generating the resulting torque; instead, they lead to stator losses and reduce the machine's efficiency, as in[25], [26]. In order to transition from the static reference frame (α, β) to the revolving reference frame (d, q), we utilize the subsequent matrix, as in (13).

$$T_r = \begin{pmatrix} \cos\theta & \sin\theta \\ -\,sin\,\theta & cos\,\theta \end{pmatrix} \tag{13}$$

Within the (d, q) subspace, the electrical, and mechanical formulas of the motor are articulated as in (14)-(16).

$$\begin{pmatrix} V_d \\ V_q \end{pmatrix} = \begin{pmatrix} R_s & 0 \\ 0 & R_s \end{pmatrix} \begin{pmatrix} i_d \\ i_q \end{pmatrix} + \frac{d}{dt} \begin{pmatrix} \Psi_d \\ \Psi_q \end{pmatrix} + \frac{d\theta}{dt} \begin{pmatrix} -\Psi_q \\ \Psi_d \end{pmatrix} \tag{14}$$

$$\begin{pmatrix} \Psi_d \\ \Psi_q \end{pmatrix} = \begin{pmatrix} L_d & 0 \\ 0 & L_q \end{pmatrix} \begin{pmatrix} i_d \\ i_q \end{pmatrix} + \sqrt{3} \begin{pmatrix} \Psi_{PM} \\ 0 \end{pmatrix} \tag{15}$$

$$C_{em} = p\left(i_q \Psi_d - i_d \Psi_q\right) \tag{16}$$

While p is the number of the pole pairs.

3. RESEARCH METHOD

3.1. Designing the power supply system for DTP-PMSM

The DTP operational condition of the switches within the two inverters is described by six Boolean control variables, denoted as Si (where i represents a, b, c, a', b', and c'). Each Si represents the idealized state of a switch, as seen in the inverter arm [27]. Specifically:

- $S_i = 1$ when the high switch is activated, and the bottom switch is deactivated
- $S_i = 0$ when the high switch is deactivated, and the bottom switch is activated

The motor phase voltages are illustrated based on the switch states in the following fashion, as in (17).

$$\begin{pmatrix} V_a \\ V_b \\ V_c \\ V_{a\prime} \\ V_{b\prime} \\ V_{c\prime} \end{pmatrix} = \frac{E}{3} \begin{pmatrix} 2 & -1 & -1 & 0 & 0 & 0 \\ -1 & 2 & -1 & 0 & 0 & 0 \\ -1 & -1 & 2 & 0 & 0 & 0 \\ 0 & 0 & 0 & 2 & -1 & -1 \\ 0 & 0 & 0 & -1 & 2 & -1 \\ 0 & 0 & 0 & -1 & -1 & 2 \end{pmatrix} \begin{pmatrix} S_a \\ S_b \\ S_c \\ S_{a\prime} \\ S_{b\prime} \\ S_{c\prime} \end{pmatrix} \tag{17}$$

While (S = Sa, Sb, Sc, Sa', Sb', and Sc') denote the switch positions, E is the DC bus electric potential.

By utilizing the transformation matrix T and tracking the switch states, we generate a total of 64 vectors in the two axis-components, namely (α, β) and (z_1, z_2). Within these vectors, 4 of them are depicted as zero vectors in Figures 2 and 3 [28]. Based on the figures, the active voltage elements within the (α,β) plane exhibit a decomposition into 4 distinct dodecagons characterized by varying magnitudes (specifically, D1, D2, D3, and D4, arranged from the innermost to the outermost dodecagon). These magnitudes are expressed in (18).

$$\begin{cases} * \, U_{D1} = \dfrac{\sqrt{(2-\sqrt{3})}}{\sqrt{3}} E \\ * \, U_{D2} = \dfrac{1}{\sqrt{3}} E \\ * \, U_{D3} = \dfrac{\sqrt{2}}{\sqrt{3}} E \\ * \, U_{D4} = \dfrac{\sqrt{(2+\sqrt{3})}}{\sqrt{3}} E \end{cases} \tag{18}$$

The voltage elements with the highest amplitude on the (α, β) plane correspond to minimum amplitudes within the (z_1, z_2) subspace, while the remaining vectors maintain their original magnitudes.

3.2. Conventional DTC for DTP-PMSM

The conventional DTC strategy represents a control method that enables the separate and decoupled regulation of stator flux and torque using a voltage inverter, as in Figure 4. This approach finds extensive application in drives for permanent magnet synchronous motors. By independently managing stator flux and torque, it becomes possible to achieve exceptional dynamic performance and precise motor control. The selection of the top 12 vectors with the highest magnitudes effectively divides the (α, β) plane in 12 distinct sectors, as illustrated in Figure 5. The indicated strategy ensures the selection of vectors with the least significance in the (z_1, z_2) plane, there by maximizing the utilization of the DC power source.

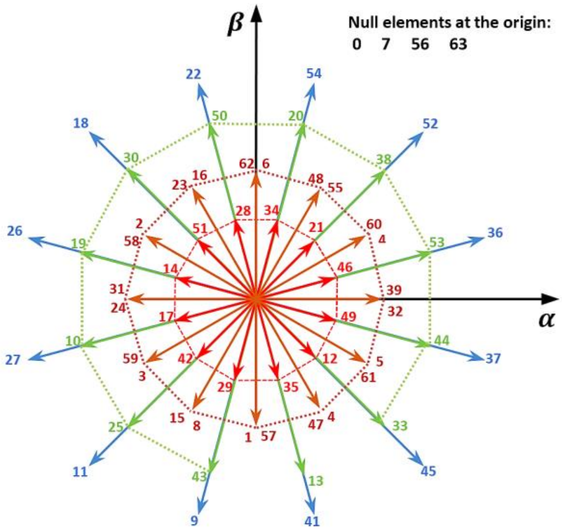

Figure 2. Diagram illustrating space vectors in the (α-β) plan

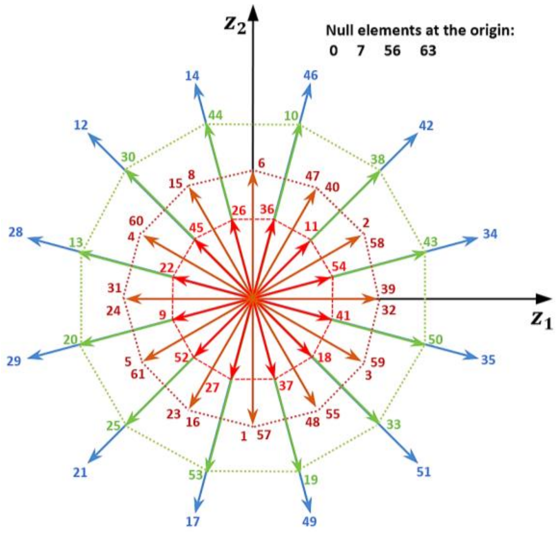

Figure 3. Diagram illustrating space vectors in the $(z_1 - z_2)$ plan

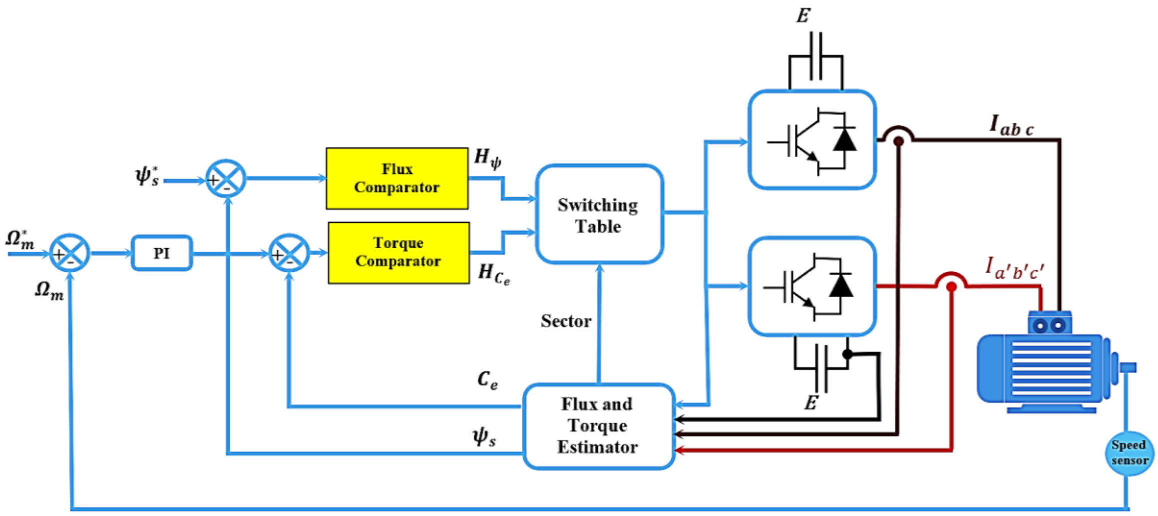

Figure 4. DTC block diagram for DTP-PMSM

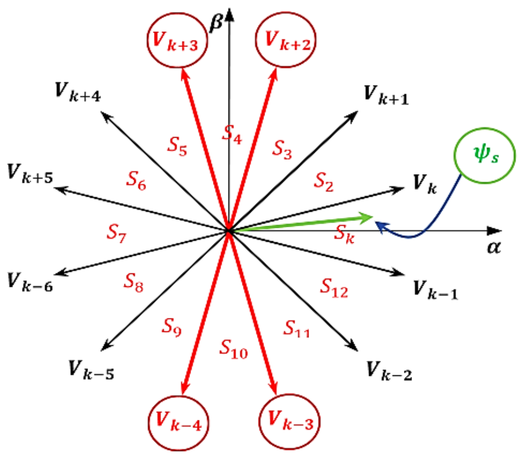

Figure 5. Distribution of sectors and selected voltage vectors for sector k

According to the principles of DTC, the maintenance of torque and flux within specified hysteresis bands necessitates the selection of an appropriate voltage during each sampling interval. This determination relies on the current error between the flux and torque values [27]. The (α, β) plane is partitioned into 12 sectors, designated as "sector k" (k = 1, ..., 12), with each sector corresponding to a specific flux vector. The initial sector encompasses an angle range of -15° to +15° degrees. The label k (k = 1, ..., 12) denotes the stator flux's positional zone, and it is determined in conventional DTC using (19). Table 1 displays the voltages to be administered when the flux is positioned within sector k, and it also outlines the adjustments required for both torque and flux. Meanwhile, Table 2 provides the prescribed command signals for flux and torque, identified as H_{ψ} and H_{Ce}, respectively.

$$(2k - 3)\pi/12 < \theta < (2k - 1)\pi/12 \quad (19)$$

Table 1. Conventional DTC switch's table

	K Sector					
H_{C_e}	10-1			10-1		
H_{ψ}		1			0	
Applied vector	V_{k+2}	V_{zero}	V_{k-3}	V_{k+3}	V_{zero}	V_{k-4}

Table 2. Hysteresis comparators –DTC-DTP-PMSM

Signal	Value	Condition
H_{C_e}	1	$C_e^* - C_e \geq \varepsilon_{Ce}$
	0	$C_e^* - C_e = 0$
	-1	$C_e^* - C_e \leq \varepsilon_{Ce}$
H_{ψ}	1	$\psi_s^* - \psi_s \geq \varepsilon_{\psi}$
	0	$\psi_s^* - \psi_s \leq \varepsilon_{\psi}$

4. THE APPROACH OF MODIFIED DTC

The proposed modified DTC technique achieves a reduction in current harmonics by specifically curtailing currents within the subspace defined by (z_1, z_2). This approach consists of modifying conventional DTC in two steps. First step is altering the switching table while retaining the use of twelve sectors, as in the conventional DTC, involves implementing a new distribution of the sectors, as depicted in Figure 6. Instead of the initial sector spanning from -15° to +15°, we reposition it counterclockwise by 15°, resulting in the selection of 0° to 30° for the first sector as shown in Figure 7. Table 3 provides information on the voltage values that should be used when the flux is within sector k. These values account for adjustments needed for both torque and flux.

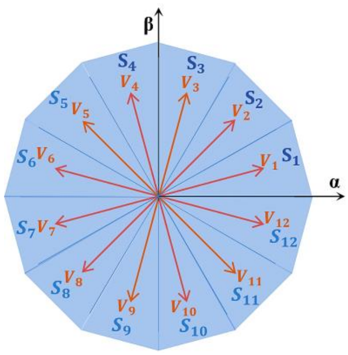

Figure 6. New distribution of sectors within (α-β)

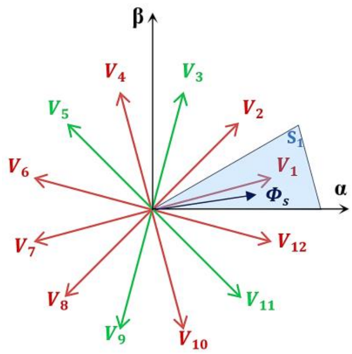

Figure 7. Choice related to vectors on sector 1

Table 3. Modified DTC switch's table (first step)

	K Sector					
H_{ψ}		1			0	
H_{C_e}	1	0	-1	1	0	-1
Applied vector	V_{k+2}	V_{zero}	V_{k-2}	V_{k+4}	V_{zero}	V_{k-4}

Second step is replacing the voltage vectors in the switching table obtained above by the voltage groups which are organized within the (α, β) subspace into twelve distinct groups, designated as {G1, G2..., G12}. Every group comprises three non-zero voltage elements extending towards the outermost dodecagon and belonging to the three adjacent sectors; for example, instead of opting for the V_{36} vector alone, we opt for a combination of vectors V_{45}, V_{37}, and V_{36}. These vectors collectively form what we refer to as group G1, as depicted in Figure 8. Figure 9 provides a visual representation of the position of these vectors within the subspace (z_1, z_2). Notably, the application duration of these vectors is carefully adjusted to ensure that their combined weighted vector sum cancels out within the subspace (z_1, z_2). As a result, precise control of the current within the subspace (z_1, z_2) leads to a decrease in current harmonics. The subsequent equation outlines the time allotted for each vector, as in (20).

$$\begin{cases} T_1 V_{45(z1z2)} + T_2 V_{36(z1z2)} + T_3 V_{37(z1z2)} = \vec{0} \\ T_1 + T_2 + T_3 = T_s \end{cases} \tag{20}$$

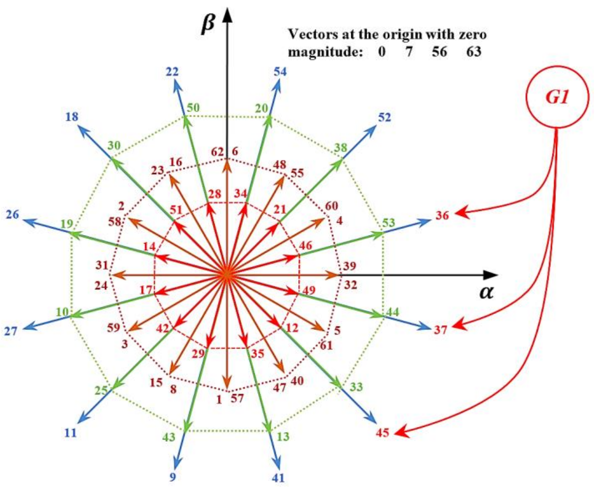

Figure 8. Voltage group G1 in (α-β)

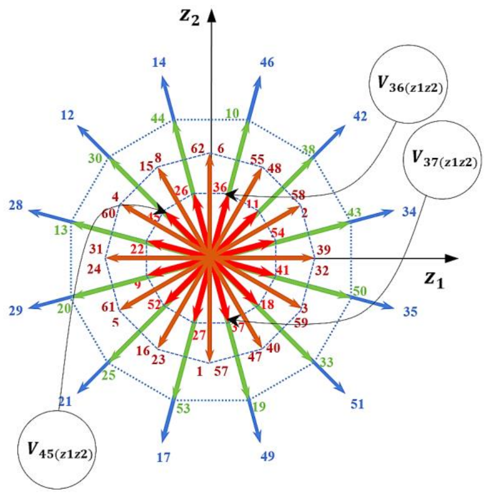

Figure 9. Vectors V_{36} , V_{37} and V_{45} in (z_1, z_2)

In which: T_s represents appraisal period. The computation of the time values yields, as in (21).

$$\begin{cases} T_1 = \left(2 - \sqrt{3}\right) \cdot T_s = T_3 \\ T_2 = \left(2\sqrt{3} - 3\right) \cdot T_s \end{cases} \tag{21}$$

The suggested method involves substituting 12 vectors obtained by Table 3 with a composite set of vectors, as illustrated in Table 4.

Table 4. Synthetic vectors employed in modified DTC

Modified DTC (first step)	Groups	Modified DTC (second step)
V_{36}	*G1: (V_{45},V_{37},V_{36})*	$T_1V_{45} + T_2V_{36} + T_3V_{37}$
V_{52}	*G2: (V_{37},V_{36},V_{52})*	$T_1V_{37} + T_2V_{52} + T_3V_{36}$
V_{54}	*G3: (V_{36},V_{52},V_{54})*	$T_1V_{36} + T_2V_{54} + T_3V_{52}$
V_{22}	*G4: (V_{52},V_{54},V_{22})*	$T_1V_{52} + T_2V_{22} + T_3V_{54}$
V_{18}	*G5: (V_{54},V_{22},V_{18})*	$T_1V_{54} + T_2V_{18} + T_3V_{22}$
V_{26}	*G6: (V_{22},V_{18},V_{26})*	$T_1V_{22} + T_2V_{26} + T_3V_{18}$
V_{27}	*G7: (V_{18},V_{26},V_{27})*	$T_1V_{18} + T_2V_{27} + T_3V_{26}$
V_{11}	*G8: (V_{26},V_{27},V_{11})*	$T_1V_{26} + T_2V_{11} + T_3V_{27}$
V_9	*G9: (V_{27},V_{11},V_9)*	$T_1V_{27} + T_2V_9 + T_3V_{11}$
V_{41}	*G10: (V_{11},V_9,V_{41})*	$T_1V_{11} + T_2V_{41} + T_3V_9$
V_{45}	*G11: (V_9,V_{41},V_{45})*	$T_1V_9 + T_2V_{45} + T_3V_{41}$
V_{37}	*G12: (V_{41},V_{45},V_{37})*	$T_1V_{41} + T_2V_{37} + T_3V_{45}$

5. RESULTS FROM SIMULATIONS AND DISCUSSION

The simulations were conducted within the MATLAB/Simulink environment, maintaining a consistent load torque of 8N.m and a steady motor speed of 300 rpm. Both approaches for DTP-PMSM, namely conventional DTC and modified DTC, was simulated, and the outcomes are depicted in Figures 10-16. Key motor properties are listed in the Table 5 [13].

Table 5. Key motor properties

Designation	Value/ unit
D.C line electric potential: E	50 V
Resistance of stator:R_s	1.09 Ω
direct-axis inductance:L_d	2.142 Mh
quadrature-axis inductance: L_q	2.142 mH
Flux by the permanent magnet:Ψ_{PM}	0.0734 Wb
Moment of inertia:J	89.10^{-3} kg.m^2
Overall coefficient of viscous friction:f	0.01 N.m.s/rad
Pole pair count: p	5

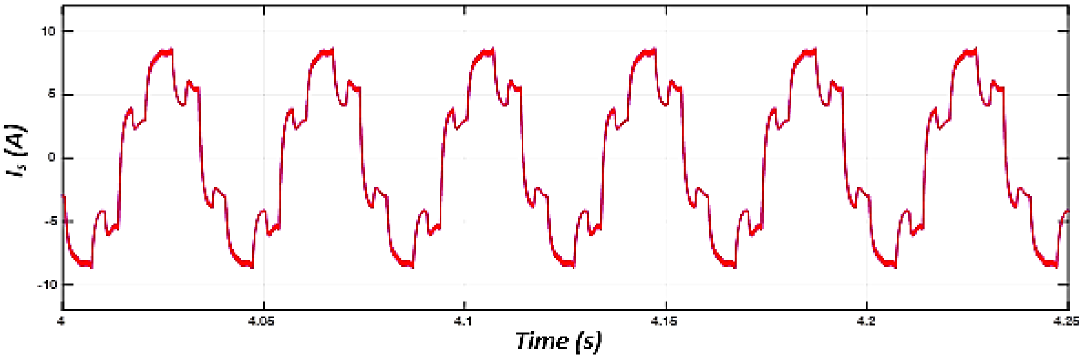

Figure 10. Current related to stator phase: conventional DTC

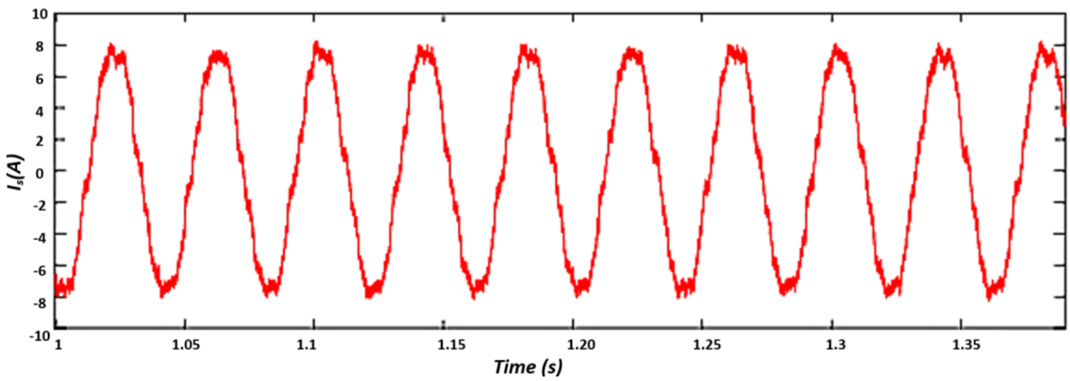

Figure 11. Current related to stator phase: modified DTC

Figure 10 illustrates that when employing the conventional DTC strategy, the phase current exhibits a non-sinusoidal form. Figure 11 demonstrates that the phase current associated with the suggested DTC strategy closely resembles a sinusoidal form. The analysis of harmonic currents related to conventional DTC shows a significant presence of the 5^{th} and 7^{th} harmonics, which are the predominant contributors to total harmonic distortion (THD) = 29.79%, as depicted in Figure 12.

In Figure 13, the harmonic assessment of the current reinforces the observation that harmonic components have been notably reduced, resulting in a THD equal to 7.74%. This reduction in harmonic currents is primarily attributed to the modified DTC method's ability to manage current elements within the (z_1, z_2) plane. This factor accounts for the observed decrease in harmonic content.

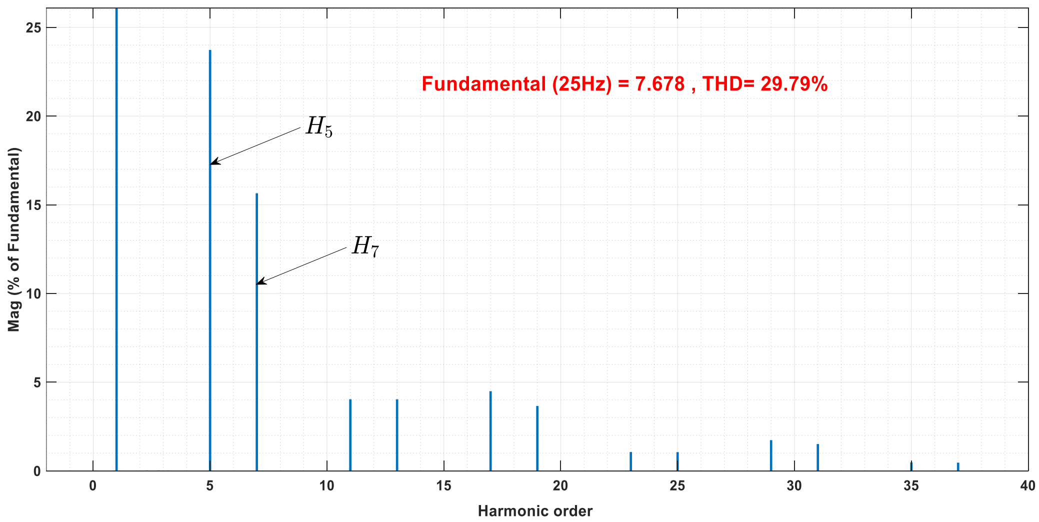

Figure 12. Spectrum related to stator phase: conventional DTC

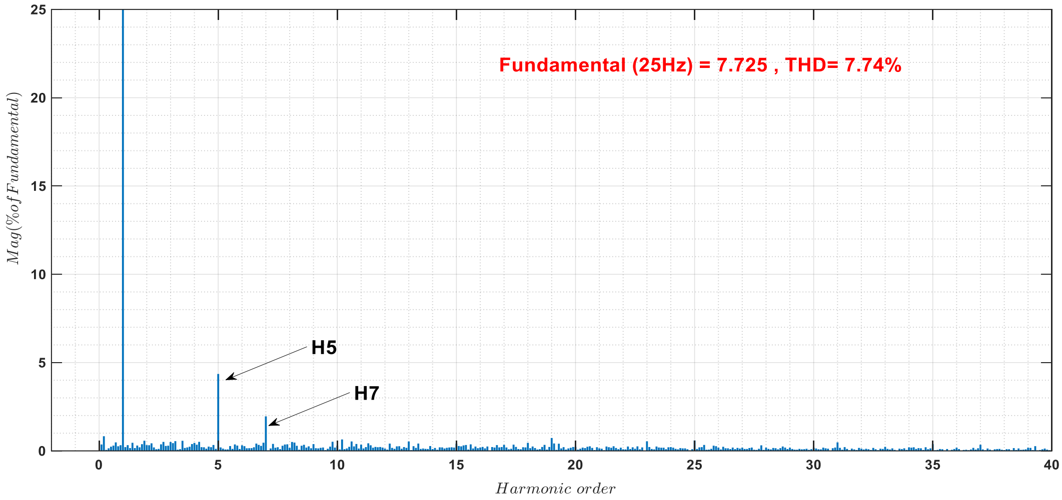

Figure 13. Spectrum related to stator phase: modified DTC

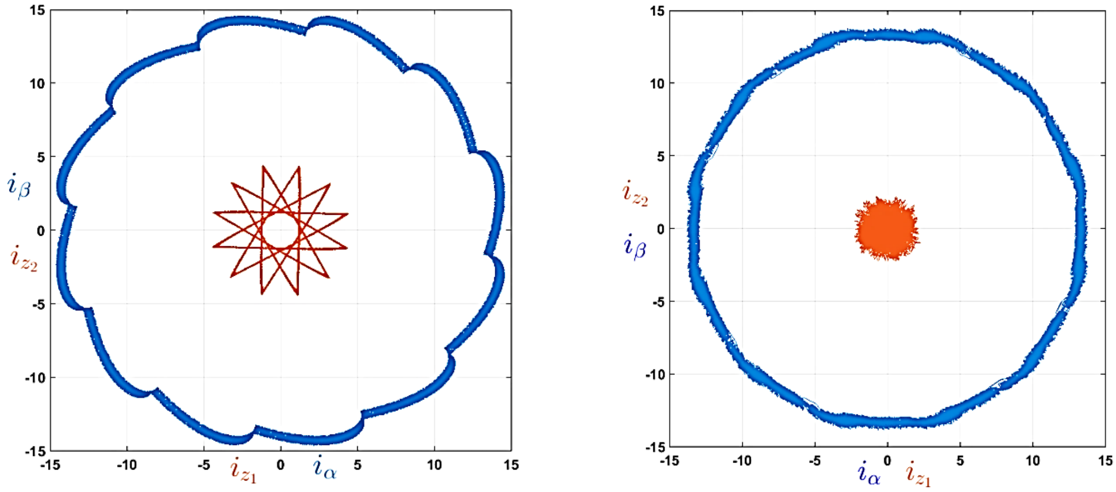

(a) (b)

Figure 14. The (α,β) and (z1,z2) current: (a) conventional DTC and (b) modified DTC

Both Figures 14(a) and 14(b) represent currents in the (α, β) and (z_1, z_2) planes, showing: i) Minimal ripple in the (z_1, z_2) plane for the proposed modified DTC; and ii) Consistent trajectories in the (α, β) plane for both employed methods. Figure 15(a) illustrates that the conventional DTC approach exhibits more pronounced flux undulations compared to the modified DTC approach, which shows a smoother flux, as depicted in Figure 15(b). In Figure 16(a), the torque exhibits an identical profile for both strategies. The presence of these harmonics does not impact the performance of the torque. Figure 16(b), the graph illustrates the response of motor's speed, with the rate of motion achieving its reference value while demonstrating strong stationary and moving characteristics.

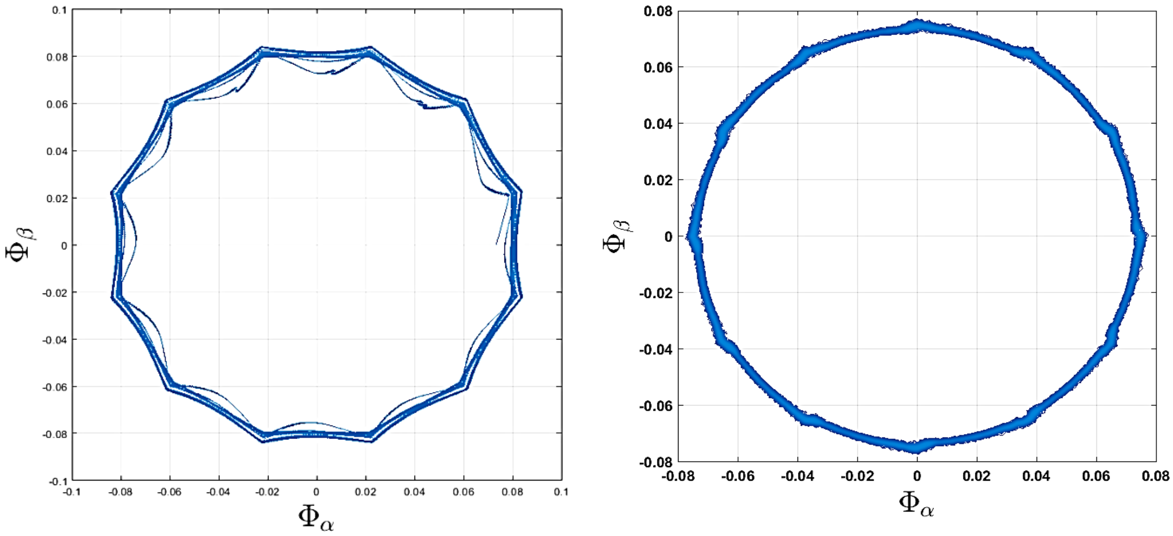

(a) (b)

Figure 15. Flux of stator phase: (a) conventional DTC and (b) modified DTC

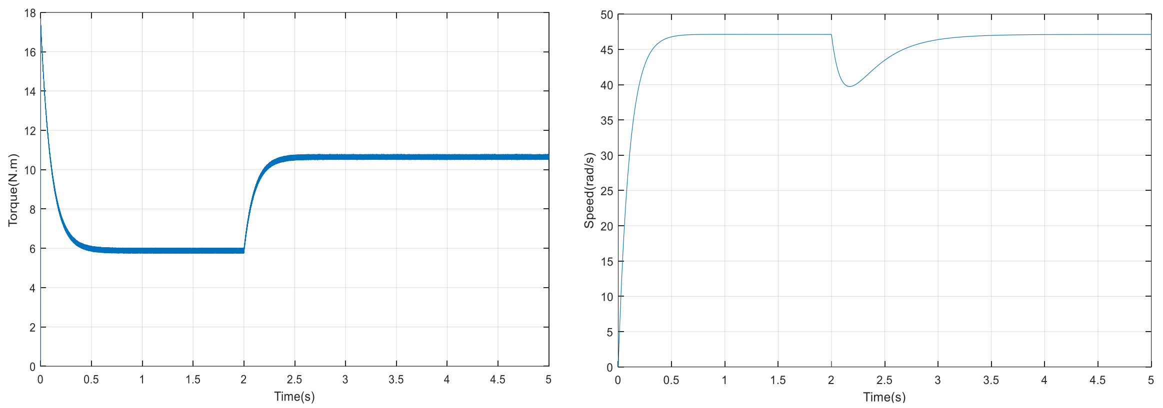

(a) (b)

Figure 16. Response of the torque and the speed for both strategies: (a) response of the torque and (b) response of the speed

6. CONCLUSION

Direct torque control represents a prominent strategy employed in high-performance electrical drive systems. In the case of DTP-PMSM, conventional DTC introduces noticeable harmonic currents. Specifically, with conventional DTC, control is focused solely on variables within the (α, β).

This article introduces a modified DTC approach for governing the DTP-PMSM. The primary objective of this strategy is to mitigate the presence of harmonics in the armature current. It achieves this by adapting a new distribution of the sectors and employing the 12 synthetic voltage vectors. This innovative technique enables to select the optimal inverter electric tension element, facilitating control within the (α, β) subspace likewise reducing currents in the (z_1, z_2) plane. Simulated data have demonstrated that this modified strategy is more effective at minimizing stator harmonic currents compared to the conventional approach, as a result, it allows for enhancing the motor efficiency.

REFERENCES

[1] M. Hasoun, A. El Afia, K. Chikh, M. Khafallah, and K. Benkirane, "A PWM strategy for dual three-phase PMSM using 12-sector vector space decomposition for electric ship propulsion," in *2018 19th IEEE Mediterranean Electrotechnical Conference (MELECON)*, May 2018, pp. 243–248. doi: 10.1109/MELCON.2018.8379101.

[2] Y. Guo and X. Yan, "Research on matrix converter control multi-phase PMSM for all electric ship," in *2011 International Conference on Electrical and Control Engineering*, Sep. 2011, pp. 3120–3123. doi: 10.1109/ICECENG.2011.6057186.

[3] H. Echeikh, R. Trabelsi, H. Kesraoui, A. Iqbal, and M. F. Mimouni, "Torque ripples improvement of direct torque controlled five-phase induction motor drive using backstepping control," *International Journal of Power Electronics and Drive Systems (IJPEDS)*, vol. 11, no. 1, pp. 64–74, Mar. 2020, doi: 10.11591/ijpeds.v11.i1.pp64-74.

[4] N. M. Max, N. Y. J. Maurice, E. Samuel, M. C. Jordan, A. Biboum, and B. Laurent, "DTC with fuzzy logic for multi-machine systems: traction applications," *International Journal of Power Electronics and Drive Systems (IJPEDS)*, vol. 12, no. 4, pp. 2044–2058, Dec. 2021, doi: 10.11591/ijpeds.v12.i4.pp2044-2058.

[5] M. Rezal and D. Ishak, "Performance evaluation of multi-phase permanent magnet synchronous motor based on different winding configurations and magnetization patterns," *International Journal of Power Electronics and Drive Systems (IJPEDS)*, vol. 10, no. 3, pp. 1197–1206, Sep. 2019, doi: 10.11591/ijpeds.v10.i3.pp1197-1206.

[6] D. Dujic, A. Iqbal, and E. Levi, "A space vector PWM technique for symmetrical six-phase voltage source inverters," *EPE Journal*, vol. 17, no. 1, pp. 24–32, Mar. 2007, doi: 10.1080/09398368.2007.11463639.

[7] Y. Yu, L. Gao, Y. Liu, and F. Chai, "24-Sector space vector decomposition for a dual three-phase PMSM," in *2014 17th International Conference on Electrical Machines and Systems (ICEMS)*, Oct. 2014, pp. 1601–1606. doi: 10.1109/ICEMS.2014.7013733.

[8] I. Takahashi and T. Noguchi, "A new quick-response and high-efficiency control strategy of an induction motor," *IEEE Transactions on Industry Applications*, vol. IA-22, no. 5, pp. 820–827, Sep. 1986, doi: 10.1109/TIA.1986.4504799.

[9] Y. A. Chapuis, D. Roye, and S. Courtine, "Commande directe du couple d'une machine asynchrone par le contrôle direct de son flux statorique (Direct torque control of an asynchronous machine by direct control of its stator flux)," *Journal de Physique III*, vol. 5, no. 6, pp. 863–880, Jun. 1995, doi: 10.1051/jp3:1995165.

[10] Z. Q. Zhu, Y. Ren, and J. Liu, "Improved torque regulator to reduce steady-state error of torque response for direct torque control of permanent magnet synchronous machine drives," *IET Electric Power Applications*, vol. 8, no. 3, pp. 108–116, Mar. 2014, doi: 10.1049/iet-epa.2013.0180.

[11] Y. Gao and L. Parsa, "Modified direct torque control of five-phase permanent magnet synchronous motor drives," in *APEC 07 - Twenty-Second Annual IEEE Applied Power Electronics Conference and Exposition*, Feb. 2007, pp. 1428–1433. doi: 10.1109/APEX.2007.357704.

[12] Y. Ren and Z. Q. Zhu, "Enhancement of steady-state performance in direct torque controlled dual-three phase permanent magnet synchronous machine drives with modified switching table," *IEEE Transactions on Industrial Electronics*, vol. 62, no. 6, pp. 3338–3350, 2014, doi: 10.1109/TIE.2014.2376881.

[13] A. El Afia, M. Hasoun, M. Khafallah, and K. Benkirane, "Efficiency improvement of dual three-phase permanent magnet synchronous motor using modified switching table DTC for electric ship propulsion," *International Journal of Power Electronics and Drive Systems (IJPEDS)*, vol. 12, no. 3, pp. 1315–1325, Sep. 2021, doi: 10.11591/ijpeds.v12.i3.pp1315-1325.

[14] K. D. Hoang, Y. Ren, Z. Zhu, and M. Foster, "Modified switching-table strategy for reduction of current harmonics in direct torque controlled dual-three-phase permanent magnet synchronous machine drives," *IET Electric Power Applications*, vol. 9, no. 1, pp. 10–19, Jan. 2015, doi: 10.1049/iet-epa.2013.0388.

[15] P. Pillay and R. Krishnan, "Modeling, simulation, and analysis of permanent-magnet motor drives. I. The permanent-magnet synchronous motor drive," *IEEE Transactions on Industry Applications*, vol. 25, no. 2, pp. 265–273, 1989, doi: 10.1109/28.25541.

[16] B. K. Bose, *Power electronics and ac drives*. 1986.

[17] J. Yang, G. Yang, and T. Li, "Direct torque control for dual three-phase PMSM based on three-phase decomposition SVPWM," in *2010 International Conference on Electrical and Control Engineering*, Jun. 2010, pp. 3655–3658. doi: 10.1109/iCECE.2010.892.

[18] Yifan Zhao and T. A. Lipo, "Space vector PWM control of dual three-phase induction machine using vector space decomposition," *IEEE Transactions on Industry Applications*, vol. 31, no. 5, pp. 1100–1109, 1995, doi: 10.1109/28.464525.

[19] M. Hasoun, A. El Afia, M. Khafallah, and K. Benkirane, "Experimental implementation PWM strategy for dual three-phase PMSM using 12-sector vector space decomposition applied on electric ship propulsion," *International Journal of Power Electronics and Drive Systems (IJPEDS)*, vol. 11, no. 4, pp. 1701–1710, Dec. 2020, doi: 10.11591/ijpeds.v11.i4.pp1701-1710.

[20] Z. Wang, J. Chen, M. Cheng, and Na Ren, "Vector space decomposition based control of neutral-point-clamping (NPC) three-level inverters fed dual three-phase PMSM drives," in *IECON 2016 - 42nd Annual Conference of the IEEE Industrial Electronics Society*, Oct. 2016, pp. 2988–2993. doi: 10.1109/IECON.2016.7793845.

[21] Z. Wang, Y. Wang, J. Chen, and Y. Hu, "Decoupled vector space decomposition based space vector modulation for dual three-phase three-level motor drives," *IEEE Transactions on Power Electronics*, vol. 33, no. 12, pp. 10683–10697, Dec. 2018, doi: 10.1109/TPEL.2018.2811391.

[22] L. Yuan, M. Chen, J. Shen, and F. Xiao, "Current harmonics elimination control method for six-phase PM synchronous motor drives," *ISA Transactions*, vol. 59, pp. 443–449, Nov. 2015, doi: 10.1016/j.isatra.2015.09.013.

[23] V. Oleschuk, V. Ermuratskii, and F. Barrero, "Combined PWM control of multi-inverter installation with two DC-links," in *2015 International Conference on Electrical Drives and Power Electronics (EDPE)*, Sep. 2015, pp. 94–98. doi: 10.1109/EDPE.2015.7325276.

[24] H. Zhang, S. Luo, Y. Yu, and L. Liu, "Study on series control method for dual three-phase PMSM based on space vector pulse width modulation," *International Journal of Control and Automation*, vol. 8, no. 1, pp. 197–210, Jan. 2015, doi: 10.14257/ijca.2015.8.1.18.

[25] K. Marouani, L. Baghli, D. Hadiouche, A. Kheloui, and A. Rezzoug, "A new PWM strategy based on a 24-sector vector space decomposition for a six-phase VSI-fed dual stator induction motor," *IEEE Transactions on Industrial Electronics*, vol. 55, no. 5, pp. 1910–1920, May 2008, doi: 10.1109/TIE.2008.918486.
[26] M. Hasoun, A. E. Afia, and M. Khafallah, "Performance comparison of two-SVPWM-strategies based vector space decomposition controlled dual three-phase PMSM for electric ship propulsion," in *2019 7th International Renewable and Sustainable Energy Conference (IRSEC)*, Nov. 2019, pp. 1–8. doi: 10.1109/IRSEC48032.2019.9078209.
[27] M. Hasoun, A. El afia, and M. Khafallah, "Field oriented control of dual three-phase PMSM based vector space decomposition for electric ship propulsion," in *2019 International Conference of Computer Science and Renewable Energies (ICCSRE)*, Jul. 2019, pp. 1–6. doi: 10.1109/ICCSRE.2019.8807703.
[28] K. Marouani, F. Khoucha, A. Kheloui, L. Baghli, and D. Hadiouche, "Study and simulation of direct torque control of double-star induction motor drive," in *2006 12th International Power Electronics and Motion Control Conference*, Aug. 2006, pp. 1233–1238. doi: 10.1109/EPEPEMC.2006.4778571.

BIOGRAPHIES OF AUTHORS

Fouad Labchir was born in Morocco in 1969. He received the Engineering degree in 1993 from Navy Royal School, Military Navy, Casablanca, Morocco; and the certificate of Navy Safety in 1994 at Cherbourg, France. Since 1994, he held positions as head of technical services or head of training services within various units, except for the year 2000 and the year 2013 when he underwent continuous training. His current research interests are in the application of power electronics converters and motor drives for electric propulsion systems. He can be contacted at email: labchirfouad69@gmail.com.

Aziz El Afia received B.Sc., M. Sc. degrees from Hassan II University, Casablanca in 1990, 1994 respectively and the Ph.D. degree in Electrical Engineering from The National High School of Electrical and Mechanical Engineering (ENSEM), Hassan II University, Casablanca in 2009. Since 2011 he has been working as a Professor of Power Electronic at the National High School of Arts and Crafts of Casablanca (ENSAM). His current research interests are in power electronics converters and control of machines and drives for application from automotive to renewable energy. He can be contacted at email: aziz.elafia@univh2c.ma.

Karim Benkirane was born in Morocco in 1960. He received B.Sc., M.Sc., and Doctorate degrees from Mohamed V University Rabat and University of Sciences and Technics at Languedoc (USTL), France, in 1978, 1983 and 1986 respectively, all in Electronics Engineering. In 1987 he joined the Royal Navy School (ERN), Casablanca, Morocco, where he is currently professor tutor in the Department Research. His main research interests the application of power electronics converts and motor drives. He has published a lot of research papers in international journals. He can be contacted at email: karbenkirane@yahoo.fr.

Mohamed Khafallah was born in Morocco in 1964. He received B.Sc., M.Sc. and Doctorate degrees from Hassan II University, Casablanca, in 1989, 1991, and 1995 respectively, all in Electrical Engineering. In 1995 he joined the National High School of Electricity and Mechanics (ENSEM), Hassan II University, Casablanca, Morocco, where he is currently professor tutor in the Department Electrical Engineering and chief of Laboratory Energy and Electrical Systems (LESE). His main research interests the application of power electronics converts and motor drives. He has published a lot of research papers in international journals, conference proceedings as well as chapters of books. He can be contacted at email: m.khafallah@gmail.com.